Int. J. Heat Mass Transfer. Vol. 27, No. 10, pp. 1893–1902, 1984
Printed in Great Britain

0017 9310/84 $3.00 + 0.00

Natural convection in a vertical porous enclosure with internal heat generation

M. HAAJIZADEH, A. F. OZGUC and C. L. TIEN
Department of Mechanical Engineering, University of California, Berkeley, CA 94720, U.S.A.

(*Received* 8 *August* 1983 *and in revised form* 6 *January* 1984)

Abstract—A theoretical study is performed on steady natural convection inside a rectangular porous enclosure with uniform internal heat generation and cooling from the side walls. For low Rayleigh numbers, the problem is tackled by regular expansion in the Rayleigh number and the resulting Poisson equations are sequentially solved by the modified Galerkin method. For large Rayleigh numbers, the boundary layer equations valid near the vertical walls along with the core region equations are examined using the Gill linearization method. The analytical predictions agree well with the numerical solutions based on the power-law difference representation of the full governing equations.

1. INTRODUCTION

NATURAL convection in porous media, induced by internal heat generation arises in various physical problems such as heat removal from nuclear fuel debris in nuclear reactors, underground disposal of radioactive waste materials, and exothermic chemical reactions in packed-bed reactors. Moreover, this phenomenon can be encountered during the storage of agricultural products where heat is generated as a result of metabolism of the products [1]. Existing analyses on this phenomenon focused mostly on the case of a horizontal porous layer with uniform heat generation and cooling at the horizontal boundaries [2]. In contrast, there appear to be no studies on the case of a porous enclosure with uniform heat generation and cooling from the side walls, although, in the above-mentioned engineering systems, lateral cooling can play a dominant role in the convection process within a heat generating porous medium. Indeed, few studies have been reported on the corresponding natural convection problem in a vertical enclosure filled with a heat generating fluid [3].

In the present work, the physics of natural convection in a vertical porous enclosure with uniform heat generation and side-wall cooling, is examined theoretically. The analysis consists of asymptotic solutions for small and large Rayleigh numbers and numerical solutions of the full governing equations. The results show some interesting features in the bicellular convective motion and the heat removal from the side walls.

2. FORMULATION OF THE PROBLEM

The model configuration and the coordinate system (x, y) are shown in Fig. 1. The flow is assumed to be steady and two-dimensional (2-D). The horizontal walls of length d are insulated and the vertical walls of height h are at uniform temperature T_w. Constant volumetric heat generation S has been assumed. Invoking Darcy's law along with the Boussinesq approximation and neglecting thermal dispersion, the dimensionless form of the governing equations and boundary condtions are

$$\partial^2\psi/\partial x^2 + \partial^2\psi/\partial y^2 = -R\,\partial T/\partial x \quad (1)$$

$$u\,\partial T/\partial x + v\,\partial T/\partial y = \partial^2 T/\partial x^2 + \partial^2 T/\partial y^2 + 1 \quad (2)$$

$$u = \partial\psi/\partial y; \quad v = -\partial\psi/x \quad (3)$$

$$\psi = 0, \quad T = 0 \quad \text{on} \quad x = 0, 1 \quad (4a)$$

$$\psi = 0, \quad \partial T/\partial y = 0 \quad \text{on} \quad y = 0, A. \quad (4b)$$

In the above equations the variables are reduced to dimensionless form by introducing the following scales

$$x, y = (x', y')/d; \quad u, v = (u', v')d/\alpha; \quad \psi = \psi'/\alpha$$

$$T = (T' - T_w)/(Sd^2/k);$$

$$R = \beta g S \kappa d^3/\alpha\nu k; \quad A = h/d \quad (5)$$

where primes denote dimensional variables, u' and v' are the Darcy velocity components in the x' and y'

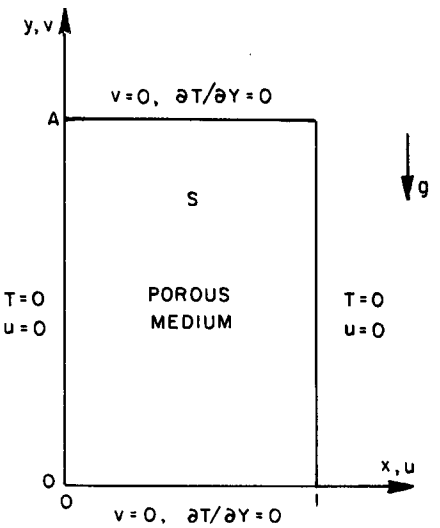

FIG. 1. Schematic diagram of the 2-D vertical porous enclosure.

NOMENCLATURE

A	aspect ratio, h/d	β	coefficient of volume expansion
$B_0, B_1, \ldots, B_{12}$	constants	$\gamma, \varepsilon, \sigma, \omega$	characteristic roots, constants
C, D	constants	δ	boundary-layer length scale
d	width	δ_e	exponential boundary-layer thickness
g	gravitational acceleration	η	horizontal stretched coordinate
h	height	θ	normalized temperature or vertical velocity, equation (48)
j	dummy index	κ	permeability
k	effective thermal conductivity	λ	exponential decay rate
n	dummy index	ν	kinematic viscosity
N	Nusselt number	ρ	fluid density
R	Rayleigh number, $\beta g S \kappa d^3/\alpha \nu k$	τ	any dimensionless variable u, v, ψ or T
S	uniform volumetric heat generation rate	ϕ	approximate function
T	temperature	ψ	stream function
T_{max}	peak temperature	ψ_0, ψ_1, ψ_2	perturbation stream functions.
T_w	cold walls temperature		
$T_0, T_1, T_2, \ldots$	temperature perturbation functions	Subscripts	
ΔT	temperature difference scale	c	pertaining to the core region
u, v	horizontal and vertical velocities	max	maximum.
x, y	horizontal and vertical distances.		
		Superscripts	
Greek symbols		$\bar{}$	η averaged
α	effective thermal diffusivity		dimensional quantities.

directions, ψ' is the stream function, T' the temperature, R the Rayleigh number and A the aspect ratio. The symbols α, β, g, κ, ν and k denote the effective thermal diffusivity, the coefficient of thermal expansion, the gravitational acceleration, the permeability, the kinematic viscosity and the effective thermal conductivity, respectively.

Local dimensionless heat transfer is characterized by the local Nusselt number defined as

$$N = 2(\partial T/\partial x)_{x=0}. \tag{6}$$

Owing to the symmetry of the problem, the vertical centerline is a stagnation streamline dividing the flow into two cells which are mirror images of each other. Consequently the present results can be employed as well for a 2-D porous enclosure cooled at only one vertical wall with other walls insulated.

3. LOW RAYLEIGH NUMBER SOLUTIONS

Regular perturbation solutions for this problem can be obtained by expanding the dependent variables ψ and T in power series of R

$$\psi = \sum_{n=0}^{\infty} R^n \psi_n(x, y) \tag{7}$$

$$T = \sum_{n=0}^{\infty} R^n T_n(x, y). \tag{8}$$

It can be easily shown that

$$T_0 = -x^2/2 + x/2 \tag{9}$$

$$\psi_0 = 0. \tag{10}$$

Thus the expansion is about the pure conduction mode.

Substitution of equations (7) and (8) into equations (1)–(3) and collection of like power terms lead to a sequence of linear equations for the successive ψ_n and T_n. For $n \geqslant 1$

$$\nabla^2 \psi_n = -\partial T_{n-1}/\partial x \tag{11}$$

$$\nabla^2 T_n = \sum_{j=0}^{n} \left(\frac{\partial \psi_j}{\partial y} \frac{\partial}{\partial x} - \frac{\partial \psi_j}{\partial x} \frac{\partial}{\partial y} \right) T_{n-j}. \tag{12}$$

By using the modified Galerkin method [4], the above series of Poisson equations are sequentially reduced to ordinary differential equations.

An approximate solution for ψ_1 can be sought in the form

$$\psi_1(x, y) = \phi(x) f(y) \tag{13}$$

where $\phi(x)$ is a function chosen *a priori* which satisfies boundary conditions

$$\phi(x) = 0 \quad \text{on} \quad x = 0, 1. \tag{14}$$

Using equation (13) with the variational equation corresponding to the Poisson equation yields

$$\int_0^1 (\nabla^2 \psi_1 + \partial T_0/\partial x) \phi(x) \, dx = 0. \tag{15}$$

For the present problem, $\phi(x)$ may be obtained by integrating equation (11) written for $n = 1$ as

$$\psi_1(x) \simeq \phi(x) = (2x^3 - 3x^2 + x)/12. \tag{16}$$

Substitution of $\psi_1(x, y)$ with the above $\phi(x)$ into equation (15) results in an ordinary differential equation for $f(y)$. After using the boundary conditions at $y = 0, A$, the approximate solution for ψ_1 can be obtained as

$$\psi_1(x,y) = [\mathrm{sh}\gamma(y-A) - \mathrm{sh}\gamma y + \mathrm{sh}\gamma A](2x^3 - 3x^2 + x)/12\mathrm{sh}\gamma A. \quad (17)$$

The solutions for T_1, ψ_2 and T_2 can be found by the same procedure as

$$T_1(x,y) = B_0\left\{\frac{\gamma}{\mathrm{sh}\varepsilon A}[\mathrm{ch}\varepsilon(y-A) - \mathrm{ch}\varepsilon y] - \frac{\varepsilon}{\mathrm{sh}\gamma A}[\mathrm{ch}\gamma(y-A) - \mathrm{ch}\gamma y]\right\} \times (-8x^6 + 24x^5 - 25x^4 + 10x^3 - x)/1440 \quad (18)$$

$$\psi_2(x,y) = \left[\left(B_1\frac{\mathrm{ch}\varepsilon A - 1}{\mathrm{sh}\varepsilon A} + B_2\frac{\mathrm{ch}\gamma A - 1}{\mathrm{sh}\gamma A}\right) \times \frac{\mathrm{sh}\sigma(y-A) + \mathrm{sh}\sigma y}{\mathrm{sh}\sigma A} + B_1\frac{\mathrm{ch}\varepsilon(y-A) - \mathrm{ch}\varepsilon y}{\mathrm{sh}\varepsilon A} + B_2\frac{\mathrm{ch}\gamma(y-A) - \mathrm{ch}\gamma y}{\mathrm{sh}\gamma A}\right] \times (-16x^7 + 56x^6 - 70x^5 + 35x^4 - 7x^2 + 2x)/20160 \quad (19)$$

$$T_2(x,y) = \left\{\left(B_3\frac{\mathrm{ch}\gamma A - 1}{\mathrm{sh}\gamma A} + B_4\frac{\mathrm{ch}\varepsilon A - 1}{\mathrm{sh}\varepsilon A}\right) \times \left[\frac{\mathrm{ch}\sigma(y-A) + \mathrm{ch}\sigma y}{\mathrm{sh}\sigma A}\right] + B_5\left[\frac{\mathrm{sh}\gamma(y-A) - \mathrm{sh}\gamma y}{\mathrm{sh}\gamma A}\right] + B_6\left[\frac{\mathrm{sh}\varepsilon(y-A) - \mathrm{sh}\varepsilon y}{\mathrm{sh}\varepsilon A}\right] + B_7\left[\frac{\mathrm{sh}\gamma(y-A) - \mathrm{sh}\gamma y}{\mathrm{sh}\gamma A}\right] \times \left[\frac{\mathrm{sh}\varepsilon(y-A) - \mathrm{sh}\varepsilon A}{\mathrm{sh}\varepsilon A}\right] + B_8\left[\frac{\mathrm{ch}\gamma(y-A) - \mathrm{ch}\gamma y}{\mathrm{sh}\gamma A}\right] \times \left[\frac{\mathrm{ch}\varepsilon(y-A) - \mathrm{ch}\varepsilon A}{\mathrm{sh}\varepsilon A}\right] + B_9\left[\frac{\mathrm{sh}\gamma(y-A) - \mathrm{sh}\gamma y}{\mathrm{sh}\gamma A}\right]^2 + B_{10}\left[\frac{\mathrm{ch}\gamma(y-A) - \mathrm{ch}\gamma A}{\mathrm{sh}\gamma A}\right]^2 + \left(B_{11}\frac{\mathrm{ch}\gamma A - 1}{\mathrm{sh}\gamma A} + B_{12}\frac{\mathrm{ch}\varepsilon A - 1}{\mathrm{sh}\varepsilon A}\right) \times \left[\frac{\mathrm{ch}\omega(y-A) + \mathrm{ch}\omega y}{\mathrm{sh}\omega A}\right]\right\} \times (448x^{10} - 2240x^9 + 4410x^8 - 4200x^7 + 1470x^6 + 882x^5 - 155x^4 + 420x^3 - 35x)/5.08 \times 10^7. \quad (20)$$

In the above equations γ, ε, σ and ω are the characteristic roots of the ordinary differential equations corresponding to ψ_1, T_1, ψ_2 and T_2, respectively, and the constants $B_0, B_1, \ldots, B_{12}$ are functions of the above characteristic roots. The values of these characteristic roots and constants are as follows

$\gamma = 6.481$; $\varepsilon = 3.362$; $\sigma = 6.893$; $\omega = 3.407$

$B_0 = 0.710$; $B_1 = -6.035$;

$B_2 = 20.555$; $B_3 = -45.793$

$B_4 = 13.445$; $B_5 = -61.348$;

$B_6 = -1818.606$; $B_7 = 3.563$

$B_8 = 3.904$; $B_9 = 5.075$;

$B_{10} = -8.167$; $B_{11} = -22.916$

$B_{12} = -1832.722$.

The perturbation functions ψ_1, T_1, ψ_2 and T_2 are depicted, for an aspect ratio of 2, on Fig. 2. In all these graphs the streamlines and isotherms are equally spaced. The conduction temperature profile (T_0) induces a bicellular flow which is symmetric along the mid-height [Fig. 2(a)]. Carrying cold fluid to the lower part of the enclosure, this bicellular motion removes the generated heat upward, thus the temperature in this region falls below the pure conduction temperature. On the other hand, for the upper half of the enclosure the fluid is already hot and can not remove heat effectively, therefore, the temperature rises above the pure conduction temperature. Figure 2(b) shows that T_1 is anti-symmetric with respect to the mid-height, positive in the upper half and negative in the lower half of the enclosure. The second-order stream function ψ_2 has four identical cells which are symmetric with respect to the center of the enclosure; it enhances the flow at the upper half and weakens it at the lower half of the enclosure. The second-order temperature T_2 has two positive parts adjacent to the top and the bottom of the enclosure, while it is negative in the core.

Although obtaining the solutions beyond T_2 is straightforward, the analysis is not carried further as the algebra becomes quite cumbersome.

4. BOUNDARY-LAYER ANALYSIS

This section deals with the case of convection at large Rayleigh numbers, driven by boundary-layer flows

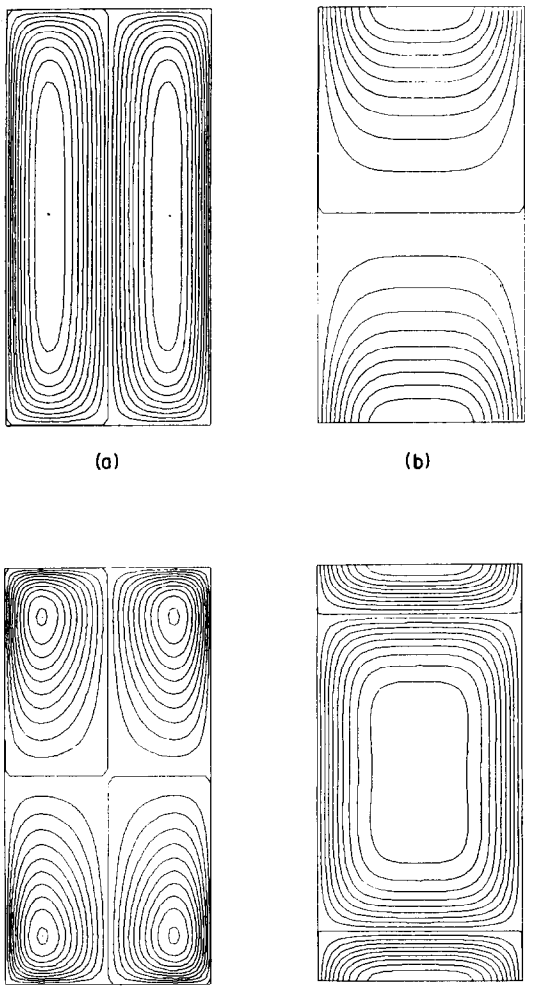

FIG. 2. Perturbation functions patterns: (a) ψ_1, $|\psi_{1\max}| = 8.0 \times 10^{-3}$; (b) T_1, $T_{1\max} = 0.287 \times 10^{-3}$ at $x = 0.5$ and $y = 2$, $T_{1\min} = -0.287 \times 10^{-3}$ at $x = 0.5, y = 0$; (c) ψ_2, $|\psi_{2\max}| = 0.86 \times 10^{-5}$; (d) T_2, $T_{2\max} = 0.409 \times 10^{-6}$ at $x = 0.5$ and $y = 0, 2$, $T_{2\min} = -0.39 \times 10^{-6}$ at $x = 0.5$ and $y = 1$. The streamlines and isotherms are equally spaced between the maximum and minimum values.

lining on the cold vertical walls. Owing to the symmetry only the LHS boundary layer is considered here. As the Rayleigh number tends toward infinity the heat generated in the enclosure is carried upward mainly by convection and heat transfer by conduction becomes important only in thin boundary layers lining on the walls. In this limit, the nominal temperature difference across the boundary layers can be estimated by noting that the total heat generated inside the enclosure should be removed across the boundary layers of thickness δ, thus

$$\Delta T \sim Sd\delta/2k. \tag{21}$$

The length scale δ for the boundary-layer thickness and the characteristic vertical velocity in the boundary layer can be obtained from equation (1) balancing the Darcy resistance and buoyancy forces in the boundary layer, and from equation (2) assuming a balance of convection and conduction in the boundary layer

$$\delta \sim d(2A)^{1/3}R^{-1/3} \tag{22}$$

$$v \sim \alpha h \delta^{-2}. \tag{23}$$

In view of the above equations, the scaling in the core is taken to be

$$x = 2x'/d; \quad y = y'/h; \quad u_c = u'\delta/\alpha$$
$$v_c = v'\delta d/2\alpha h; \quad T_c = (T' - T_w)/\Delta T. \tag{24}$$

Substituting the above variables into the stream function and energy equations and taking the limit $R \to \infty$ yield the following governing equations in the core region

$$\partial T_c/\partial x = 0 \tag{25}$$

$$v_c\, \partial T_c/\partial y = 1 \tag{26}$$

where the subscript c indicates the core values. From the above equations it follows that $T_c = T_c(y)$ and $v_c = v_c(y)$. These unknown functions should be found through the consideration of the side-wall boundary layers.

By employing the stretched variables for x and v as

$$\eta = x(R/16A)^{1/3}; \quad v = v_c(R/16A)^{-1/3} \tag{27}$$

in the stream function and energy equations and taking the limit $R \to \infty$ the field equations for the LHS boundary layer become

$$\partial v/\partial \eta = \partial T/\partial \eta \tag{28}$$

$$u\, \partial T/\partial \eta + v\, \partial T/\partial y = \partial^2 T/\partial \eta^2 \tag{29}$$

with the conditions

$$u = 0, \quad T = 0 \quad \text{on} \quad \eta = 0$$
$$v \to v_c, \quad T \to T_c, \quad \eta \to \infty. \tag{30}$$

Note that the internal heat generation effect on the boundary layer is of the order of $R^{-1/3}$ so it vanishes as $R \to \infty$. Therefore, the above equations become identical to those of an isothermal wall in a thermally stratified porous medium. However, in the present problem the stratification is unknown and coupled to the boundary-layer equations. In order to solve the boundary-layer equations along with the corresponding core region equations, an analytical approach similar to that used by Bergholz [3] is employed. This method, which was first employed by Gill [5], is based upon linearization of the boundary-layer equations by replacing $u(\eta, y)$ and $\partial T(\eta, y)/\partial y$ with η averaged values $\bar{u}(y)$ and $\overline{\partial T(y)/\partial y}$, respectively. Combining equations (28) and (29) and using the above average values yield

$$\bar{u}\, \partial v/\partial \eta + v\, \partial \bar{T}/\partial y = \partial^2 v/\partial \eta^2. \tag{31}$$

After using the boundary conditions (30), the solution to the above ordinary differential equation whose coefficients are functions of the parameter y can be easily shown to be

$$v = -T_c\, e^{\lambda \eta} \tag{32}$$

where

$$\lambda = (u - \sqrt{(u^2 + 4\,\partial T/\partial y)})/2. \quad (33)$$

Consequently, by using equation (28), there results

$$T = T_c(1 - e^{\lambda\eta}). \quad (34)$$

Note that, due to the linearization of the boundary-layer energy equation, matching in the limit of $\eta \to \infty$ can not be used for evaluation of the unknown functions v_c and T_c; rather global mass and energy conservation is employed. These are

$$v_c = -\int_0^\infty v(\eta, y)\,d\eta \quad (35)$$

$$\frac{d}{dy}\left\{\int_0^\infty v(\eta, y)[T(\eta, y) - T_c]\,d\eta\right\} + \left.\frac{\partial T}{\partial \eta}\right|_{\eta=0} - 1 = 0. \quad (36)$$

Substitution of equations (32) and (34) into the above equations yields

$$v_c = -T_c/\lambda \quad (37)$$

$$d(T_c^2/2\lambda)/dy + \lambda T_c + 1 = 0. \quad (38)$$

Eliminating v_c from equations (26) and (37) and using equation (38) results in

$$4T_c^3 + 3CT_c^2 = D - 6y \quad (39)$$

$$\lambda = 1/(2T_c + C) \quad (40)$$

$$v_c = -T_c(2T_c + C). \quad (41)$$

The integration constants C and D could have been evaluated by matching with the solutions valid in the horizontal boundary layers [3, 4]. However, analogous to Bergholz [3] the impermeable boundary condition at the horizontal end walls is taken to be the inner solution i.e.

$$v_c = 0 \quad \text{on} \quad y = 0, 1. \quad (42)$$

Moreover, it is plausible to assume that the rising core flow at $y = 0$ has been cooled to the cold wall temperature by lateral cooling, so

$$T_c \simeq 0 \quad \text{on} \quad y = 0 \quad (43)$$

using conditions (42) and (43) the unknown constants C and D can be evaluated as

$$C = -2(3^{1/3}), \quad D = 0. \quad (44)$$

With the implicit relation for $T_c(y)$, it is possible to compute the v_c and T_c distribution in the core as well as the boundary-layer profiles for u, v and T.

Finally, the exponential boundary-layer thickness and the Nusselt number can be reckoned as

$$\delta_e = 2(3^{1/3} - T_c) \quad (45)$$

$$N(y) = T_c/2(T_c - 3^{1/3}). \quad (46)$$

5. NUMERICAL METHOD

To obtain numerical solutions to equations (1)–(3), the power-law difference form of the energy equation [6] along with the central-difference form of the stream function derivatives were solved by the successive-relaxation method. The T, ψ, u and v fields were advanced iterativelv one at a time until the following convergence criteria were all met

$$|\tau_{new} - \tau_{old}|_{max} \leqslant 10^{-6}. \quad (47)$$

Here τ represents the general field variable and max denotes the maximum value over all the grid points. A check was also made of the overall energy balance for the enclosure. For all runs reported here, the energy balance was satisfied within 2%.

For faster convergence, the energy equation was over-relaxed while the stream function equation was under-relaxed. The optimum relaxation parameters were 1.2 for T and 0.8 for ψ. Moreover, after each iteration the velocities were corrected in order to satisfy the zero net mass flow across the horizontal and vertical mesh lines.

A run with $R = 10^5$, $A = 2$ and a non-uniform grid of 81×51 points took 600 iterations to converge and 150 computing seconds on a CDC-7600 computer.

6. RESULTS AND DISCUSSION

6.1. *Low Rayleigh number solution*

In Figs. 3–6 numerically calculated and analytically predicted temperature and velocity distributions are compared for the aspect ratios of 2 and 5 and the Rayleigh numbers of 50 and 100. Characteristic temperature and vertical velocity distributions along the mid-height of the enclosure are shown in Fig. 3; the ordinate indicates the normalized values defined as

$$\theta = \frac{T(x, A/2)}{T(1/2, A/2)} = \frac{v(x, A/2) - v(0, A/2)}{v(1/2, A/2) - v(0, A/2)}. \quad (48)$$

For values of the Rayleigh number below about 100 the numerical temperature and vertical velocity profiles are

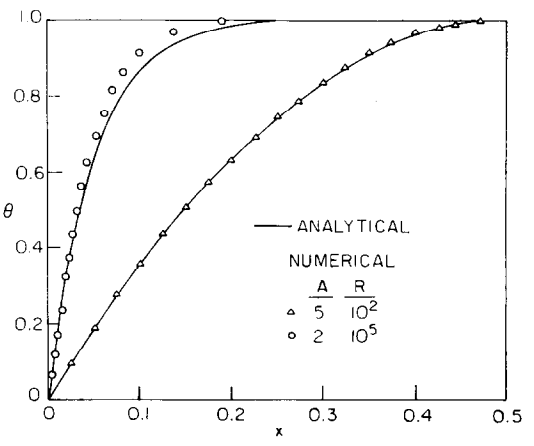

FIG. 3. Normalized temperature and vertical velocity profiles along the mid-height.

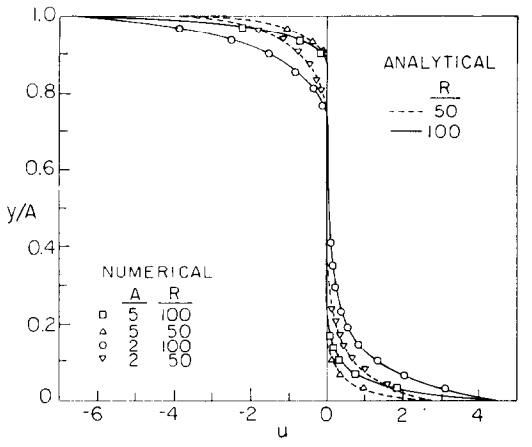

FIG. 4. Horizontal velocity profiles along $x = 0.2$.

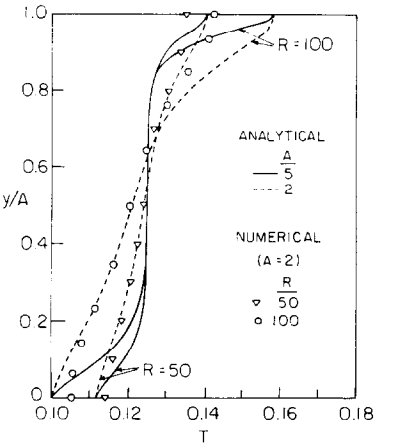

FIG. 6. Temperature profiles along the centerline.

parabolic in agreement with the analytical solutions denoted by solid lines. As the Rayleigh number increases, however, the profiles in the central region become flat and most of the temperature and velocity variations occur in thin boundary layers lining on the vertical walls. As would be expected the wall boundary layers become thinner for higher R. From Fig. 3, it is evident that the temperature and the vertical velocity profiles are similar.

Except for the regions adjacent to the top and bottom walls, the flow has a simple parallel structure, the solution for which could be obtained by setting $u = 0$ (Fig. 4) in the governing equations. In this region, the vertical velocity is constant along the vertical lines and it increases linearly with the Rayleigh number. The velocity profile along any horizontal line is parabolic similar to that shown on Fig. 3, and the temperature distribution is established by pure conduction as indicated in Fig. 6. The deviation from the parallel flow structure occurs in the top and bottom end regions where, respectively, the ascending heated flow and the descending cooled flow encounter the obstruction posed by the impermeable horizontal walls and start to turn. In these regions, as the flow approaches the horizontal walls the horizontal velocity becomes significant (Fig. 4), while the vertical velocity gradually vanishes (Fig. 5). Moreover, the temperature distribution deviates from the parabolic conduction profile, indicating the significance of the convective heat transfer in the end regions.

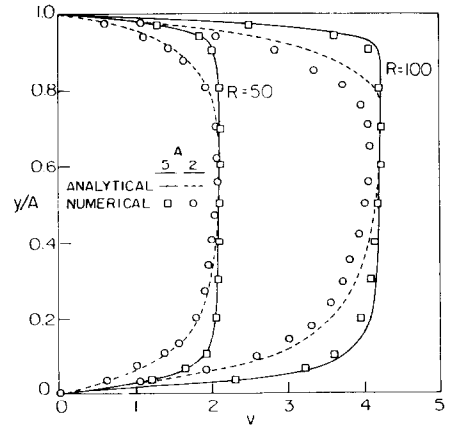

FIG. 5. Vertical velocity profiles along the vertical centerline.

It is seen that, for a fixed Rayleigh number, the horizontal velocity and temperature peaks are fixed for any aspect ratio $A \gtrsim 2$ although they are increasing functions of R. This is due to the fact that in a tall cavity with a low Rayleigh number, the vertical velocities in the parallel flow region are independent of A. Therefore, a fixed Rayleigh number yields identical end-region flows for any aspect ratio, providing that the enclosure could accommodate the end regions. Figures 4–7 indicate that as the aspect ratio decreases, the convection mode becomes relatively more important and the end regions occupy a larger portion of the enclosure, although their absolute sizes almost remain constant.

The bottom end region penetrates further into the parallel flow region with increasing Rayleigh number. On the other hand the size of the top end region is not sensitive to the variation of the Rayleigh number as seen in Figs. 4–7. Further increase of the Rayleigh number results in disappearance of the parallel flow and eventually convection becomes important throughout the cavity.

The local Nusselt number distribution for $R = 50$, depicted in Fig. 7, indicates pure conductive heat transfer along the wall with deviation from this mode in the top and bottom end regions, where the flow turns and the convective heat transfer plays an important role. This deviation becomes more significant as R increases or A decreases, and as it can be seen for $R = 100$ and $A = 2$ the pure conduction zone disappears totally due to dominant convection throughout the cavity. In the top end region where the rising hot flow turns and impinges on the cold wall, heat fluxes higher than that of the pure conduction case ensue. The converse is true for the bottom end region where the descending cold flow turns and carries away the generated heat in this region. Thus, in this region

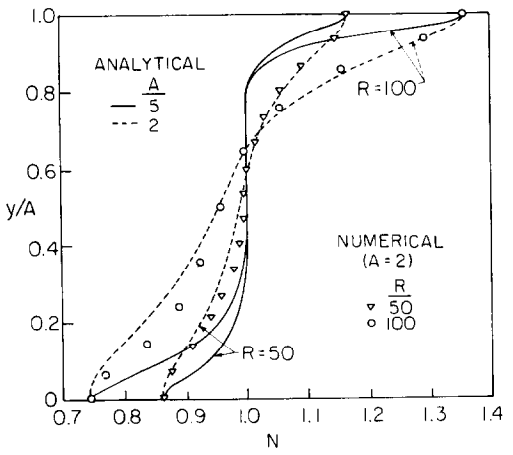

FIG. 7. Variation of the Nusselt number along the side walls.

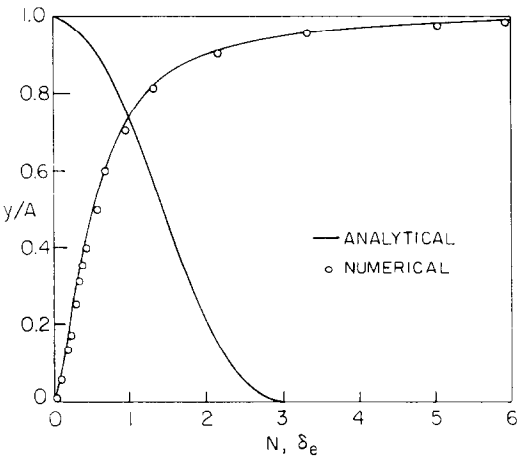

FIG. 9. Variations of the exponential boundary-layer thickness and the Nusselt number along the side walls.

the convection has a cooling effect with smaller heat fluxes compared to that of the pure conduction case.

From Figs. 3–7, it is apparent that the low Rayleigh number solutions agree quite well with the numerical results for small R, and as expected, these solutions deviate from the numerical predictions as the convection become stronger, i.e. as either R increases or A decreases.

6.2. *Boundary-layer solution*

The boundary-layer solutions in the core region along with the corresponding numerical results for $R = 5 \times 10^4$ and 10^5 with $A = 2$ are shown in Fig. 8. The numerical results indicate that the normalized vertical velocity and temperature profiles in the core are almost independent of the Rayleigh number, as expected from the boundary-layer solutions. In the bottom end region, however, the numerical vertical velocity profile has a bulge and varies slightly with the Rayleigh number. These behaviors can be explained by the fact that even for $R = 10^5$ the bottom portion of the enclosure has not entered into the boundary-layer regime and, as Fig. 10 indicates, two-tenths of the isotherms in the core are still non-stratified. This is also evident from the discrepancy existing between the numerical and analytical core temperature profiles for $y \lesssim 0.2$ depicted on Fig. 8. The vertical velocity profile indicates flow entrainment to the vertical boundary layers for $y/A > 0.5$. On the other hand, below the mid-height the flow is ejected from the boundary layers.

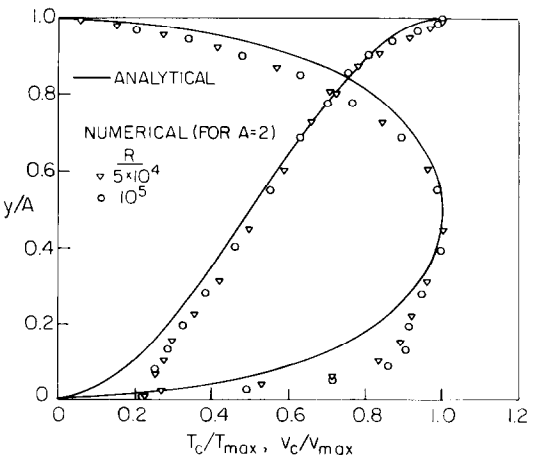

FIG. 8. Core temperature and velocity profiles.

Figure 8 shows that the core temperature is an increasing function of y thus it is always stabilizing. Neglecting the horizontal boundary layers, the core temperature profile does not satisfy the adiabatic boundary conditions at the top and bottom walls. Although it is clear that the theory and the numerical solutions are in good agreement for the temperature profile (at least for $y \gtrsim 0.2$), the analytical solutions overestimate the vertical velocity for $y/A > 0.5$ and underestimate it for $y/A < 0.5$.

The variation of the Nusselt number and the boundary-layer thickness along the vertical boundaries depicted on Fig. 9, indicate that most of the generated heat is removed along the upper part of the cold walls where the boundary layers are relatively thinner. As the flow descends along the cold walls the boundary layers become thicker; consequently the Nusselt number decreases, such that, the lower 40% of the cold walls remove only 5% of the total generated heat. Note that the analytical solutions yield zero boundary-layer thickness at $y/A = 1$, and as a result the analytical Nusselt number is singular at this point. This singularity can be removed by the consideration of the horizontal boundary layer on the top wall [3]. However, the numerical solutions indicate that $N \simeq 13.67$ at $y/A = 1$. Figure 9 indicates that the analytical method accurately predicts the heat flux variation along the vertical walls, despite the discrepancies existing between numerical and analytical core profiles.

Figure 10 shows plots of the isotherms and streamlines for an aspect ratio of 2 and different Rayleigh numbers. For $R = 10$ the almost parallel isotherms, implying the conduction dominance, induce a weak convective motion with bicellular structure. The two cells are the mirror images of each other, and they

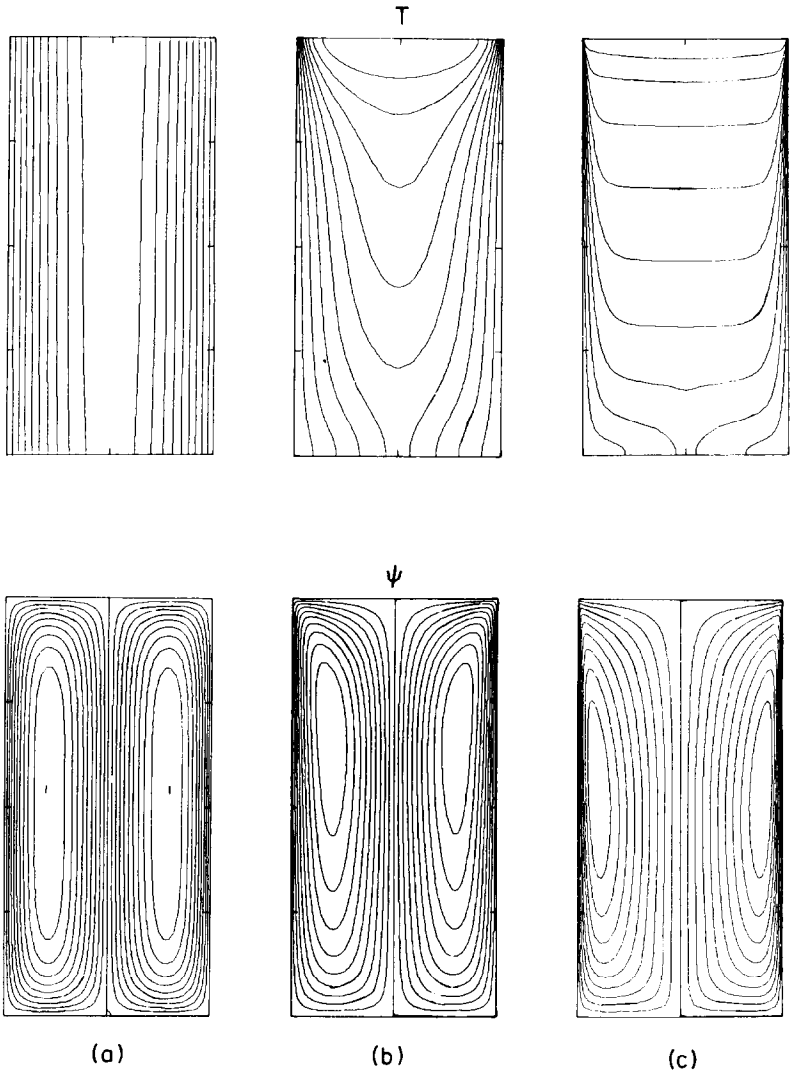

FIG. 10. Isotherms and streamlines for different values of the Rayleigh number: (a) $R = 10$, $T_{max} = 0.130$, $|\psi_{max}| = 0.078$; (b) $R = 10^3$, $T_{max} = 0.118$, $|\psi_{max}| = 4.880$; (c) $R = 10^5$, $T_{max} = 0.028$, $|\psi_{max}| = 44.348$. The increments between adjacent isotherms and streamlines are $T_{max}/10$ and $\psi_{max}/10$, respectively.

are almost symmetric with respect to the horizontal centerline. Note that the convective motion is stronger near the cold walls where the isotherms are more closely spaced (parabolic temperature distribution). As the Rayleigh number increases, stronger convective motion ensues. Consequently, near the cold walls, the isotherms become closely spaced together in the top where the ascending hot flow turns towards the cold wall, and further apart in the bottom where the descending cold flow empties into the core. Closer spacing of the isotherms at the wall is an indication of a higher heat transfer rate. The point of the maximum ψ also migrates towards the top and the flow pattern becomes more asymmetric with respect to the mid-height. For $R = 1000$ the core isotherms start to flatten at the top of the enclosure, while at the bottom they are still almost parallel to the vertical walls indicating the conduction dominance. A further increase in the Rayleigh number causes further stratification of the isotherms in the core. On the other hand, cooling occurs in thinner boundary layers and the point of maximum ψ starts to descend towards the enclosure mid-height. For $R = 10^4$ stratification is weaker and the wall boundary layers are thicker, while for $R = 10^5$ the flow shows very strong boundary-layer behavior and the cold fluid descends in thinner boundary layers. The flat isotherms in the core indicate the negligible lateral conduction and equal spacing of the streamlines implies uniform vertical velocities in the core, as predicted by the boundary-layer theory. The isothermal patterns indicate how the heat flux varies along the cold wall for different Rayleigh numbers.

Of specific interest in the engineering applications is the peak temperature in the enclosure. Figure 11 shows the variation of this quantity with the Rayleigh number for the case of $A = 2$. Note that for values of the Rayleigh number below about 300, the peak temperature is a weakly increasing function of R while

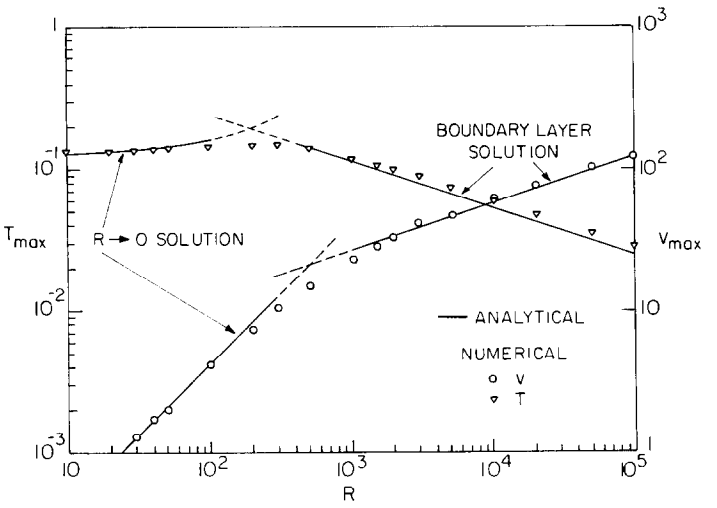

FIG. 11. Variation of the peak temperature and the peak vertical velocity with the Rayleigh number.

for $R > 300$ it drops as the Rayleigh number increases. This trend is consistent with the displacement of the cells' centers shown on Fig. 10. In the low Rayleigh number regime, as R increases, the points of maximum ψ move closer to the top wall and the available areas for direct contacts between the cold walls and the turning hot flows decrease. On the other hand, the convection becomes stronger. These two adverse effects cause the peak temperature to increase slowly with the Rayleigh number. For higher Rayleigh numbers, however, as R increases, the centers of the cells move towards the mid-height and the direct contact areas increase. At the same time the convective motion increases. Both of these result in a more efficient cooling, therefore, the peak temperature becomes a decreasing function of the Rayleigh number.

Numerically calculated and analytically predicted maximum core velocity variations with the Rayleigh number are also compared in Fig. 11, for the case of $A = 2$. The low Rayleigh number solutions are in good agreement with the numerical results for the values of the Rayleigh number below about 100. On the other hand, the boundary-layer solutions predicts the numerical results for the Rayleigh numbers above about 2000. In the intermediate regime, however, both of these theories become inadequate.

7. SUMMARY AND CONCLUDING REMARKS

The problem of natural convection in a 2-D vertical porous enclosure with uniform internal heat generation has been studied for a wide range of Rayleigh numbers. The low Rayleigh number regime is characterized by a parallel flow structure in the central region of the enclosure and two end-region flows adjacent to the top and bottom adiabatic walls. In the parallel flow region, conduction is the dominant mode of heat transfer and the temperature and vertical velocity profiles are parabolic. Conversely, in the end regions where the flow turns, the convective heat transfer becomes significant. Analogous to the case with the heat generating fluid the high Rayleigh number regime is characterized by a thermally stratified core region and two thin boundary layers lining the cold vertical walls. In the core region, the generated heat is carried upward by vertical convection and the lateral conduction is negligible, while in the boundary layers heat is removed from the descending flows by lateral cooling.

For Rayleigh numbers below about $R = 300$, as the Rayleigh number increases the centers of the bicellular circulation move up while the peak temperature increases. On the other hand, at about $R = 300$ the centers start to migrate towards the mid-height and the peak temperature starts to drop.

Finally, mention should be made of the parametric domain in which the analytical solutions are acceptable. The upper bound on R, for which the low Rayleigh number solutions are valid, can be found by noting that the zero-order temperature should be always greater than the higher order terms. Considering the point of the maximum temperature it can be shown that for $A = 2$

$$R \ll 433.$$

Comparison with the numerical results shows that these solutions are acceptable for values of the Rayleigh number below about $R = 100$. For taller enclosures, however, this upper bound is higher. On the other hand, the validity range for the boundary-layer theory can be obtained by the restriction on the boundary-layer thickness, i.e. $\delta \ll d/2$. Taking the boundary-layer thickness at $y = 0.2$, below which negligible heat transfer occurs, the above condition leads to

$$R \gg 128A.$$

The numerical result for $A = 2$ show that, for $R > 2000$, the boundary-layer theory satisfactorily predicts the peak temperature and the maximum core velocity. Note that as A increases the conduction mode becomes more dominant, therefore, the flow enters the boundary-layer regime for higher Rayleigh numbers. It should be noted that in the present study the existence

of a 2-D steady laminar flow is assumed. However, one would expect that there is an upper bound on R beyond which the flow would become unsteady or turbulent.

REFERENCES

1. K. J. Beukema, S. Bruin and J. Schenk, Three-dimensional natural convection in a confined porous medium with internal heat generation, *Int. J. Heat Mass Transfer* **26,** 451–458 (1983).
2. N. Rudraiah, B. Veerappa and S. Balachandra Rao, Effects of nonuniform thermal gradient and adiabatic boundaries on convection in porous media, *Trans. Am. Soc. Mech. Engrs*, Series C, *J. Heat Transfer* **102,** 254–260 (1980).
3. R. F. Bergholz, Natural convection of a heat generating fluid in a closed cavity, *Trans. Am. Soc. Mech. Engrs*, Series C, *J. Heat Transfer* **102,** 242–247 (1980).
4. L. V. Kantorovich and V. I. Krylov, *Approximate Methods of Higher Analysis*, pp. 304–327. Noordhoff, The Netherlands (1958).
5. A. E. Gill, The boundary-layer regime for convection in a rectangular cavity, *J. Fluid Mech.* **26,** 515–535 (1966).
6. S. Patankar, *Numerical Heat Transfer and Fluid Flow*. McGraw-Hill, New York (1980).

CONVECTION NATURELLE DANS UNE ENCEINTE POREUSE AVEC CREATION DE CHALEUR A L'INTERIEUR

Résumé—On présente une étude théorique de la convection naturelle stationnaire dans une enceinte rectangulaire poreuse avec une création de chaleur uniforme à l'intérieur et un refroidissement par les parois. Pour des nombres de Rayleigh faibles, le problème est traité par un développement en nombre de Rayleigh et les équations de Poisson résultantes sont résolues séquentiellement par la méthode de Galerkin modifiée. Pour des grands nombres de Rayleigh, les équations de couche limite valables près des parois verticales et les équations de la région du coeur sont examinées en utilisant une méthode de linéarisation. Les calculs numériques s'accordent bien avec les solutions basées sur la représentation en différence loi-puissance des équations gouvernant l'ensemble.

FREIE KONVEKTION IN EINEM VERTIKALEN PORÖSEN HOHLRAUM MIT INNEREN WÄRMEQUELLEN

Zusammenfassung—Eine theoretische Untersuchung der stationären freien Konvektion in einem rechteckigen, porösen Hohlraum mit gleichförmig verteilten inneren Wärmequellen und Kühlung an den Seitenwänden wurde durchgeführt. Für kleine Rayleigh-Zahlen wird das Problem durch reguläre Entwicklung nach der Rayleigh-Zahl behandelt, wobei die resultierenden Poissonschen Gleichungen durch die modifizierte Galerkin-Methode gelöst werden. Für große Rayleigh-Zahlen werden die an den vertikalen Wänden gültigen Grenzschichtgleichungen zusammen mit den Kerngleichungen unter Verwendung der Linearisationsmethode von Gill untersucht. Die analytischen Voraussagen stimmen gut mit den numerischen Lösungen überein.

ЕСТЕСТВЕННАЯ КОНВЕКЦИЯ В ВЕРТИКАЛЬНОЙ ПОРИСТОЙ ОБЛАСТИ С ВНУТРЕННИМ ВЫДЕЛЕНИЕМ ТЕПЛА

Аннотация—Проведено теоретическое исследование стационарной естественной конвекции внутри прямоугольной пористой замкнутой области с равномерно распределенными внутренними источниками, которая охлаждается с боковых сторон. При малых значениях числа Рэлея задача решается методом регулярных разложений по числу Рэлея, а полученные в результате уравнения Пуассона решаются затем модифицированным методом Галеркина. При больших значениях числа Рэлея уравнения пограничного слоя для области вблизи вертикальных стенок вместе с уравнениями для центральной области анализируются гилловским методом линеаризации. Результаты аналитических расчетов хорошо согласуются с численными решениями полных определяющих уравнений.